

Cove-Edged Graphene Nanoribbons with Incorporation of Periodic Zigzag-Edge Segments

Xu Wang, Ji Ma,* Wenhao Zheng, Silvio Osella, Nicolás Arisnabarreta, Jörn Droste, Gianluca Serra, Oleksandr Ivashenko, Andrea Lucotti, David Beljonne, Mischa Bonn, Xiangyang Liu, Michael Ryan Hansen, Matteo Tommasini, Steven De Feyter, Junzhi Liu,* Hai I. Wang, and Xinliang Feng*



Cite This: *J. Am. Chem. Soc.* 2022, 144, 228–235



Read Online

ACCESS |



Metrics & More



Article Recommendations



Supporting Information

ABSTRACT: Structurally precision graphene nanoribbons (GNRs) are promising candidates for next-generation nano-electronics due to their intriguing and tunable electronic structures. GNRs with hybrid edge structures often confer them unique geometries associated with exotic physicochemical properties. Herein, a novel type of cove-edged GNRs with periodic short zigzag-edge segments is demonstrated. The bandgap of this GNR family can be tuned using an interplay between the length of the zigzag segments and the distance of two adjacent cove units along the opposite edges, which can be converted from semiconducting to nearly metallic. A family member with periodic cove-zigzag edges based on $N = 6$ zigzag-edged GNR, namely 6-CZGNR-(2,1), is successfully synthesized in solution through the Scholl reaction of a unique snakelike polymer precursor (10) that is achieved by the Yamamoto coupling of a structurally flexible S-shaped phenanthrene-based monomer (1). The efficiency of cyclo-dehydrogenation of polymer 10 toward 6-CZGNR-(2,1) is validated by FT-IR, Raman, and UV–vis spectroscopies, as well as by the study of two representative model compounds (2 and 3). Remarkably, the resultant 6-CZGNR-(2,1) exhibits an extended and broad absorption in the near-infrared region with a record narrow optical bandgap of 0.99 eV among the reported solution-synthesized GNRs. Moreover, 6-CZGNR-(2,1) exhibits a high macroscopic carrier mobility of $\sim 20 \text{ cm}^2 \text{ V}^{-1} \text{ s}^{-1}$ determined by terahertz spectroscopy, primarily due to the intrinsically small effective mass ($m^*_e = m^*_h = 0.17 m_0$), rendering this GNR a promising candidate for nanoelectronics.



INTRODUCTION

Structurally defined graphene nanoribbons (GNRs) have attracted much attention in the past decade due to their intriguing electronic properties and potential applications in nanoelectronic devices.^{1–4} Two bottom-up synthetic strategies, including on-surface and in-solution methods, have been developed to achieve GNRs with precisely defined widths and edge structures (i.e., armchair, zigzag, or cove edge).^{5–8} Compared with the surface-assisted method, solution-based synthesis displays significant advantages in terms of scalability, processability, and edge functionality.^{9–11} Among various GNRs, cove-edged GNRs (CGNRs) bearing [4]helicene motifs represent an important class, as their nonplanar geometry could effectively improve the solubility and determine the unique solid-state packing structures that are not shared by the planar GNRs.^{12–15} However, the synthesis of fully CGNRs remains highly challenging due to the lack of efficient synthetic strategies and precursor design. In 2015, we demonstrated a fully cove-edged GNR consisting of bischrysenes units, which however

produced only oligomers in solution and short ribbons on the surface due to the steric hindrance at the bay positions of chrysenes that impedes the synthesis of high molecular weight polymers.¹² In addition, the synthesis of CGNRs from pyrene units also failed due to the incomplete Scholl reaction from the pyrene-based polymer precursor.¹⁶ Therefore, the development of CGNRs with new edge topology is highly desirable both for introducing novel chemical structures and for band structure engineering in designing electronic devices. Recent theoretical and experimental studies reveal that the combination of different edge structures in GNRs can provide unique geometries and

Received: August 25, 2021

Published: December 28, 2021



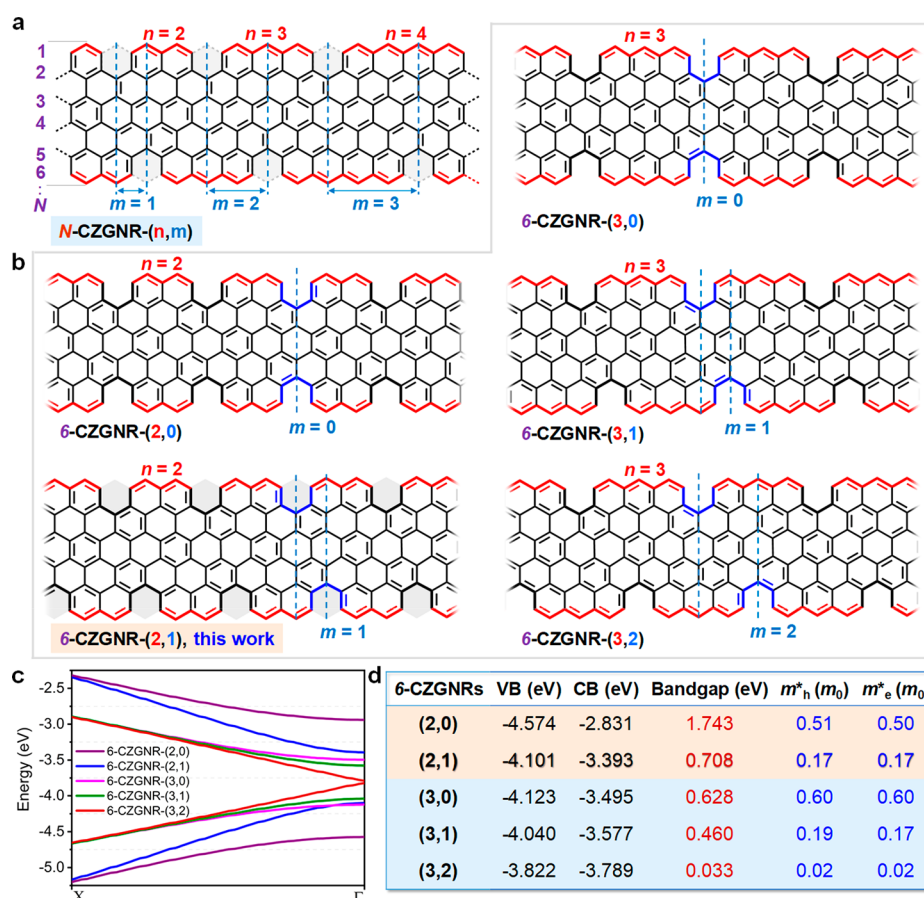


Figure 1. (a) Schematic illustration of new types of CGNRs with periodic zigzag edge segments (N -CZGNR- (n,m)). (b) The chemical structures of five examples of CGNRs based on a 6-ZGNR backbone, including the 6-CZGNR-(2,1) synthesized in this work. (c) A comparison between the band structures of the 6-CZGNRs- (n,m) in panel b. (d) The calculated valence band (VB) energy, conduction band (CB) energy, bandgap value, and the effective masses for holes (m^*_h) and electrons (m^*_e) of the 6-CZGNRs- (n,m) in panel b.

exotic electronic structures.^{17–22} As a representative example, the presence of short zigzag-edge segments in armchair-edged GNRs (AGNRs) demonstrates the possibility of realizing magnetic ordering and topological electronic states.¹⁷ Nevertheless, the synthesis of CGNRs with periodic zigzag-edge segments has remained elusive.

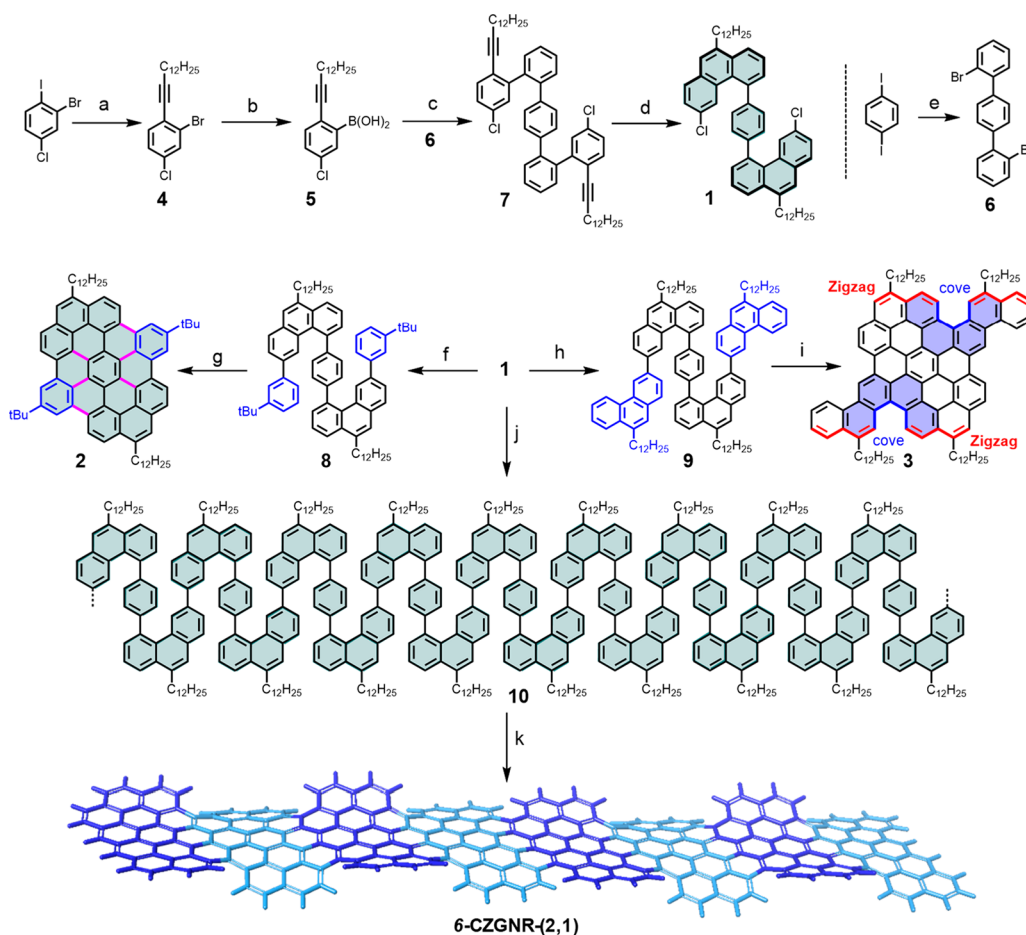
Herein, we present a new type of curved GNRs with a combination of periodic cove-zigzag edges, which can be viewed as a periodic removal of one carbon atom along the opposite edges in the corresponding fully zigzag-edged GNRs (ZGNRs). By varying the length of zigzag edges and the relative position of the cove units, a series of periodic cove-edged GNRs can be constructed, whose electronic structures can be fine-tuned from semiconducting to nearly metallic according to theoretical calculations. On the basis of this design principle, we demonstrate the first example of periodic cove-zigzag edged GNRs, namely 6-CZGNR-(2,1). The novelty of its synthesis lies in the design strategy of the snakelike polymer precursor (10) from a structurally flexible S-shaped monomer (1). The resulting 6-CZGNR-(2,1) adopts a curved conformation with alternate up–down edge topologies and possesses an average length of ~ 20 nm which is much longer than the previously reported CGNRs.^{12,15,16} The chemical structure of 6-CZGNR-(2,1) is confirmed by solid-state NMR, FT-IR and Raman analyses, as well as supported by the successful synthesis of two model compounds (2 and 3). Remarkably, the UV–vis spectrum of 6-CZGNR-(2,1) exhibits an extended absorption

into the near-infrared (NIR) region with a record-low optical bandgap of 0.99 eV among the reported solution-phase synthesized GNRs.^{20,23–25} Contact-free terahertz (THz) spectroscopy reveals high macroscopic carrier mobility of $20 \text{ cm}^2 \text{ V}^{-1} \text{ s}^{-1}$ for 6-CZGNR-(2,1). This value is among the highest for GNR films quantified by THz spectroscopies,²⁰ suggesting promising applications for optoelectronics and nanoelectronics.²⁶

RESULTS AND DISCUSSION

GNR Structure and Calculation. As illustrated in Figure 1, the regular arrangement of carbon vacancies (or cove edges) along the N -ZGNR edges provides CGNRs bearing periodic cove-zigzag segments, which are therefore denoted as N -CZGNR- (n,m) , where N specifies the width of the original ZGNR backbone, n is the number of zigzag edges between the two coves, and m is the relative position of the cove edges as indicated by the dashed lines in Figure 1a (more details for the nomenclature are presented in Supporting Information). For a given N , a variety of CGNR structures can be generated by varying n and m . We take the 6-CZGNR- (n,m) as a prototype to explore the geometries and variations in the electronic structure of the CGNRs as a function of n and m by density functional theory (DFT) calculations, see SI for details. When n is 2 or 3, five types of CGNRs can be obtained by changing the parameter m (Figure 1b). Because of the presence of the repeating [4]helicene at the edges, such CGNRs exhibit a nonplanar

Scheme 1. Synthetic Routes for the Key Monomer 1, Precursor Polymer 10, Model Compounds (2 and 3), and 6-CZGNR-(2,1) with a DFT Optimized Geometrydodecyl chains are omitted for clarity^a



^a(a) 1-Tetradecyne, Pd(PPh₃)₂Cl₂, CuI, THF, Et₃N, rt, 24 h, 88%; (b) *n*-BuLi, triisopropyl borate, THF, -78 °C, 1 h, 92%; (c) Pd(PPh₃)₄, K₂CO₃, toluene/ethanol/H₂O, 80 °C, 24 h, 60%; (d) PtCl₂, toluene, 120 °C, 48 h, 38%; (e) Pd(PPh₃)₄, (2-bromophenyl)boronic acid, K₂CO₃, toluene/ethanol/H₂O, 70 °C, 12 h, 81%; (f) Pd(OAc)₂, K₃PO₄, toluene, 80 °C, 24 h, 85%; (g) FeCl₃, CH₃NO₂, DCM, rt, 1.5 h, 91%; (h) Pd(OAc)₂, K₃PO₄, toluene, 80 °C, 24 h, 87%; (i) FeCl₃, CH₃NO₂, DCM, rt, 2 h, 88%; (j) Ni(COD)₂, COD, 2,2''-bipyridine, toluene/DMF, 80 °C, 3 days, 86%; (k) FeCl₃, CH₃NO₂, DCM, rt, 3 days, 91%. Dodecyl chains are omitted for clarity.

geometry with tilted upward and downward edge topologies. Interestingly, the electronic structure of 6-CZGNR-(*n,m*) can be tuned from semiconducting to almost semimetallic (with a tiny bandgap, e.g., down to ~0.03 eV for 6-CZGNR-(3,2)) by varying *n* and *m* (Figure 1c,d). First, by changing the *n* from 2 to 3, that is, from (2,0) to (3,0), the bands are energetically shifted almost parallel to each other, resulting in a dramatic reduction of the bandgap from 1.74 to 0.63 eV. Second, a large decrease in the bandgap is also observed. When *n* is kept fixed and *m* is changed from 0 to 3, the bandgap is found to go down from 0.63 eV for 6-CZGNR-(3,0) to 0.46 eV for 6-CZGNR-(3,1) and 0.03 eV for 6-CZGNR-(3,2), respectively.

The bandgap tuning is accompanied by effective modulation of the effective mass of charge carriers with values of $m^*_h = 0.19 m_0$ for holes and $m^*_e = 0.17 m_0$ for electrons for 6-CZGNR-(3,1) and a much smaller value of 0.02 m_0 for both electrons and holes for 6-CZGNR-(3,2). For 6-CZGNR-(2,*m*), the bandgap shows a significant decrease from 1.74 to 0.71 eV with a change of *m* from 0 to 1, and the effective mass of 6-CZGNR-(2,1) is calculated to be small with $m^*_e = m^*_h = 0.17 m_0$. Note that a small effective mass could be beneficial for achieving high charge carrier mobility (μ) by considering $\mu = e\tau/m^*$ (in a Drude-like

model, τ is the scattering time, e is the elementary charge).^{20,21} Instead of the 6-CZGNR-(3,2) with the lowest bandgap and the smallest effective masses in this GNR family, we ultimately chose the synthesis of 6-CZGNR-(2,1) as the first example of cove-edged GNR with periodic zigzag edges considering its synthetic feasibility as well as the stability issue of the semimetallic 6-CZGNR-(3,2) in solution. Moreover, 6-CZGNR-(2,1) also possesses the record low bandgap and low effective masses among the reported solution-synthesized GNRs.

Synthesis and Characterization of Model Compounds (2 and 3). The synthesis of 6-CZGNR-(2,1) is based on the S-shaped key monomer 1,4-bis(6-chloro-10-dodecylphenanthren-4-yl)benzene (1), which was obtained from the commercially available 2-bromo-4-chloro-1-iodobenzene over five steps as depicted in Scheme 1. First, 2-bromo-4-chloro-1-iodobenzene was synthesized from 2-bromo-4-chloro-1-iodobenzene via Sonogashira coupling with 1-tetradecyne in 88% yield. Then, compound 4 was transformed into (5-chloro-2-(tetradec-1-yn-1-yl)phenyl)boronic acid (5) by the lithiation reaction with *n*-BuLi at -78 °C in 92% yield. Meanwhile, compound 2,2''-dibromo-1,1':4',1''-terphenyl (6) was achieved through the Suzuki coupling of 1,4-diiodobenzene with (2-

bromophenyl)boronic acid in 81% yield. Subsequently, a Suzuki coupling between compounds **4** and **6** gave 5,5''-dichloro-2,2''-di(tetradec-1-yn-1-yl)-1,1':2',1'':4'',1''':2''',1''''-quinquephenyl (**7**) with a yield of 60%. After that, the key building block **1** was obtained from **7** in 38% yield using alkyne benzannulation with platinum(II) chloride (PtCl₂) as a catalyst. In order to examine the suitability and efficiency of the cyclodehydrogenation from phenanthrene-based precursor, two model compounds as the “cutouts” from the 6-CZGNR-(2,1), namely 2,11-di-*tert*-butyl-6,15-didodecyldibenzo[*hi,uv*]phenanthro[3,4,5,6-*bcdef*]-ovalene (**2**) and 1,4-bis(9,9'-didodecyl-[3,3'-biphenanthren]-5-yl)benzene (**3**), were prepared before the ribbon synthesis. Specifically, the corresponding phenanthrene-based oligomer precursors 1,4-bis(6-(3-(*tert*-butyl)phenyl)-10-dodecylphenanthren-4-yl)benzene (**8**) and 1,4-bis(9,9'-didodecyl-[3,3'-biphenanthren]-5-yl)benzene (**9**) were synthesized through monomer **1** by Suzuki coupling with 3-(*tert*-butyl)phenylboronic acid and 2-(9-dodecylphenanthren-3-yl)-4,4,5,5-tetramethyl-1,3,2-dioxaborolane, respectively. Remarkably, the Scholl reaction of **8** and **9** gave the model compounds **2** and **3** an excellent isolated yield (**2**, 91%; **3**, 88%) by using iron(III) chloride (FeCl₃, 3.5 equiv/H) as the Lewis acid and oxidant.²⁷ The successful formation of **2** and **3** was first confirmed by MALDI-TOF MS analysis, in which the observed isotopic distribution patterns matched well with the calculated spectra (Figure 2a). Because of the poor solubility of **2** and **3** in common organic solvents, we measured their solid-state NMR (Figures S16–17), in which the correct ratio between aliphatic and aromatic protons for both compounds were determined.

To confirm the chemical structure of model compound **3**, we conducted micro FT-IR and FT-Raman measurements and compared obtained results to DFT-calculated spectra (Figure 2b). In the IR spectrum, the analysis is restricted to the C–H out-of-plane bending region (650–1000 cm⁻¹), where significant fingerprints of the topology of polycyclic aromatic hydrocarbons and graphene molecules are found.²⁸ Clearly, the experimental IR peaks are in full accordance with the calculated IR transitions (further details are reported in the SI). The FT-Raman spectrum of **3** agrees well with the DFT results, revealing the characteristic nuclear displacement patterns of the D and G modes, as expected for graphene molecules (the representation of such nuclear displacements is reported in the SI). In particular, the weak feature observed at 1301 cm⁻¹ is a convolution of several contributions, assigned to collective D-like ring-breathing modes coupled with in-plane CH bending modes in the graphenic unit and CH₂ twisting modes in the side chains. The strong line observed at 1338 cm⁻¹ also displays a D-like nuclear displacement pattern featuring ring-breathing displacements localized at the center of the graphene molecule. The broad and structured band observed at 1604 cm⁻¹ is assigned to several computed G modes; each of them shows the characteristic ring stretching pattern with different localization and displacement direction. Thus, the observed good correspondence between the vibrational spectra simulated by DFT and the experiments supports the successful synthesis of compound **3**.

Structural studies of model compounds **2** and **3** were further carried out at the molecular level using scanning tunneling microscopy (STM) (Figure 2c,d). The self-assembly of **2** and **3** at the 1,2,4-trichlorobenzene (TCB)/highly oriented pyrolytic graphite (HOPG) interface revealed that the adsorbed long alkyl chains align along the main symmetry axes and thus define the molecular orientation. The size and shape of these features agree

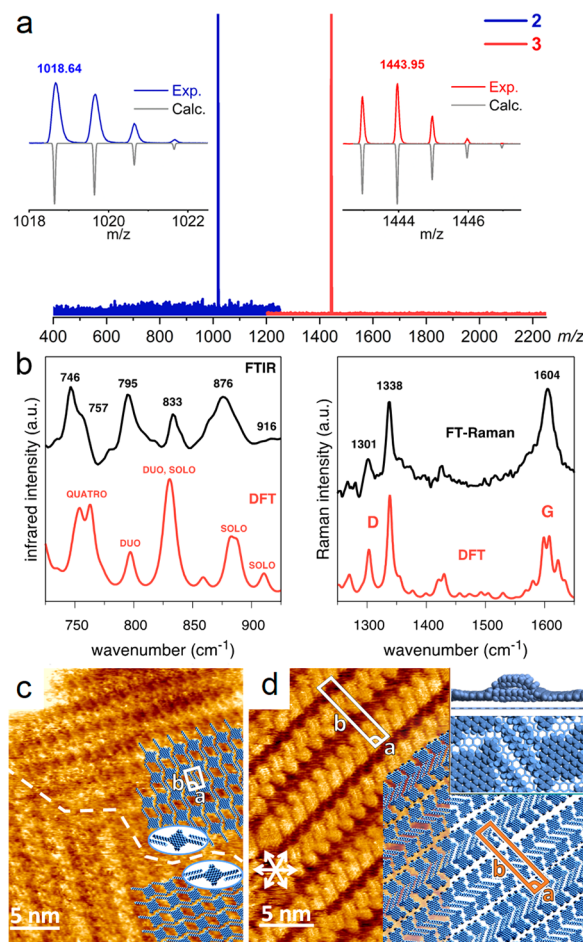


Figure 2. (a) High-resolution MALDI-TOF mass spectra of **2** and **3**. (b) Experimental and simulated FT-IR and Raman spectra of **3**. (c) STM and tentative molecular models of two enantiomeric domains formed by **2** at the TCB/HOPG interface. Unit cell: $a = 1.8 \pm 0.1$ nm, $b = 2.65 \pm 0.05$ nm, angle = $90.2^\circ \pm 0.5^\circ$. Imaging parameters: $I_{\text{set}} = 60$ pA, $U_{\text{bias}} = +0.2$ V. (d) STM and a tentative molecular model of **3** self-assembled at TCB/HOPG interface. White arrows indicate the directions of the main symmetric axes of graphite. Unit cell: $a = 1.6 \pm 0.1$ nm, $b = 7.5 \pm 0.1$ nm, angle = $89.6^\circ \pm 0.7^\circ$. Imaging parameters: $I_{\text{set}} = 850$ pA, $U_{\text{bias}} = +0.3$ V. In the overlaid molecular model, the desorbed alkyl chains are colored in violet (only the base CH₂ groups are shown). The inset in the top left corner shows a force field (MM+) optimized geometry of alkyl chains packed into a double-decker lamellar structure. For clarity, enlarged panels c and d are available in SI.

well with the simulation results for **2** and **3**, providing clear confirmation of their chemical identities. We also compared their assemblies to gain insight into intermolecular interactions that may be relevant to the nonplanar geometry. Compound **2** assembles into a chiral lamellar network in which the bulky *tert*-butyl groups space out the polyaromatic cores within the rows at 1.8 nm. As a result, each dodecyl chain has close van der Waals contact only with one other alkyl chain from the neighboring rows. Compound **3** also forms a chiral 2D network but with a much more complex structure. In a tentative molecular model, half of the alkyl chains (colored in violet) are desorbed into solution. At the same time, the remaining dodecyl groups at the zigzag sites dimerize with zigzag chains from neighboring rows similarly to **2**. The dodecyls at cove sites form a second alkyl chain layer on top of the dimerized zigzag chains (see inset in the top right corner of Figure 2d).

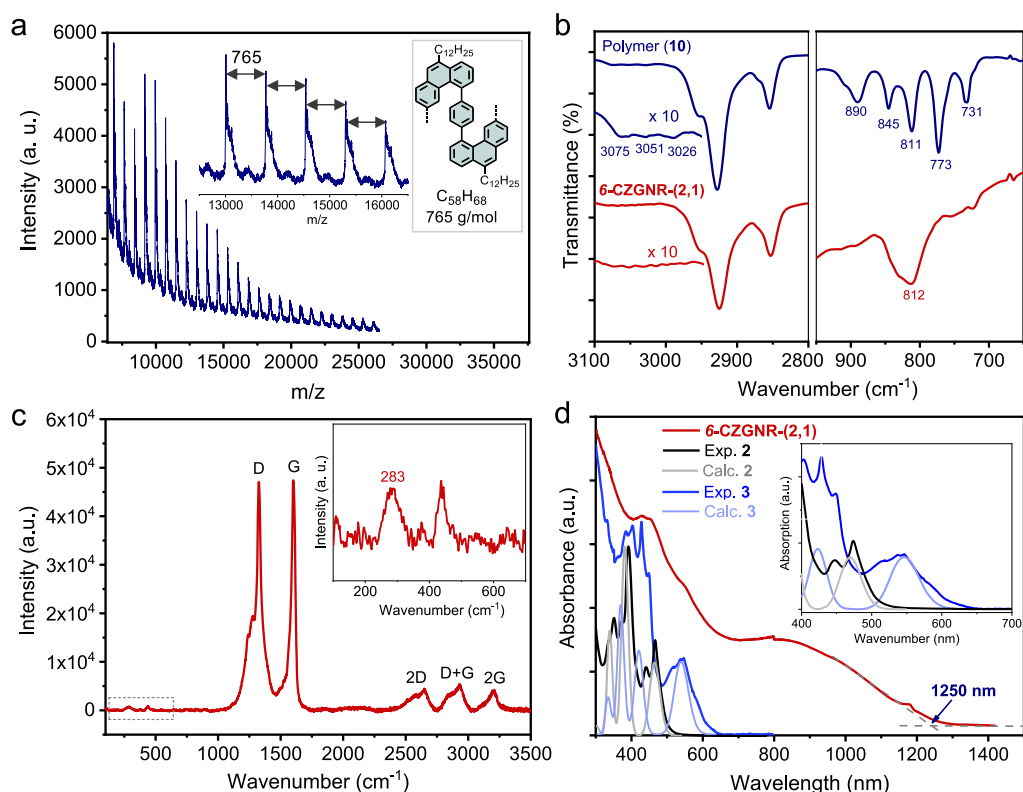


Figure 3. (a) MALDI-TOF mass spectrum of polymer precursor **10** in the linear mode. (b) FTIR spectra of **10** and **6-CZGNR-(2,1)**. (c) Raman spectrum of the **6-CZGNR-(2,1)** measured at 532 nm. (d) UV-vis absorption spectra of the **6-CZGNR-(2,1)** in NMP solution (0.1 mg mL^{-1}), and model compounds **2** and **3** in CH_2Cl_2 solution ($1 \times 10^{-5} \text{ M}$). The simulated spectra of **2** and **3** are also displayed.

Synthesis and Characterization of **6-CZGNR-(2,1)**.

Toward the synthesis of **6-CZGNR-(2,1)**, the polymerization of **1** was first performed by the AA-type Yamamoto reaction with Ni catalyst in toluene and dimethylformamide (DMF) for 3 days. The MALDI-TOF mass spectrum of the resultant snake-like poly(1,4-di(phenanthren-4-yl))benzene precursor **10** indicates that the m/z intervals are well consistent with the exact mass of the repeating unit (765 g mol^{-1}) (Figure 3a). Then, the large-molecular weight fraction of the corresponding polymer (**10**) was fractionated with the help of recycling preparative gel permeation chromatography (GPC). The analytical GPC analysis against linear polystyrene standard revealed that the number-average molecular weight (M_n) of the polymer **10** is around $24\,800 \text{ g mol}^{-1}$ with a narrow dispersity of ~ 1.2 (Figure S2). Finally, the phenanthrene-based polymer precursor **10** was “graphitized” into **6-CZGNR-(2,1)** through the Scholl reaction in dichloromethane solution with iron(III) chloride (FeCl_3 , 15 equiv/H) as the Lewis acid and oxidant. On the basis of the M_n of precursor **10**, the average length of **6-CZGNR-(2,1)** is estimated to be $\sim 20 \text{ nm}$, which is superior to other reported cove-edged GNRs.^{12,15,16} Interestingly, DFT simulation manifests that **6-CZGNR-(2,1)** with periodic cove-zigzag edges adopt a nonplanar geometry with alternate up-down conformation along the edges (Scheme 1).

The successful formation of **6-CZGNR-(2,1)** was demonstrated by FT-IR, Raman and solid-state NMR investigations. FTIR analysis of polymer **10** and **6-CZGNR-(2,1)** revealed the disappearance of the signal triad from aromatic C–H stretching vibrations at 3026 , 3051 , and 3075 cm^{-1} after the “graphitization” (Figure 3b).²⁹ In addition, out-of-plane (opla) C–H deformation bands at 731 , 773 , 811 , and 845 cm^{-1} typical for mono- and disubstituted benzene rings were attenuated. This is

accompanied by appearance of a broad peak in a range of $800\sim 850 \text{ cm}^{-1}$, which can be assigned to the opla band typical for aromatic C–H at the cove position and zigzag edge. In the Raman spectrum of **6-CZGNR-(2,1)**, an intense and sharp G-band peak and a broader D-band peak were observed at 1600 and 1324 cm^{-1} , respectively, which are typical for the GNRs with fine “graphitized” structure (Figure 3c).^{27,30,31} The rather broad D band is justified by the conformation dependence of the simulated Raman spectra (Figure S26). Meanwhile, well-resolved double-resonance signals are also observed at 2648 , 2913 , and 3197 cm^{-1} , which can be respectively assigned to 2D, D + G and 2G peaks. The frequency of the radial breathing-like mode (ν_{RBLM}) is nearly independent of the edge structure and can be estimated roughly by $\nu_{\text{RBLM}} = 3222/w \text{ cm}^{-1}$, in which $w(\text{\AA})$ is the width of the GNR.³⁰ The RBLM of **6-CZGNR-(2,1)** with a width of $w = 11.2 \text{ \AA}$ can thus be estimated to be 288 cm^{-1} , which is in good agreement with the experimental result of 283 cm^{-1} (see the inset picture in Figure 3c). Moreover, the solid-state ^1H and $^{13}\text{C}\{^1\text{H}\}$ MAS NMR experiments (Figures S18 and S19) confirm the successful cyclodehydrogenation of polymer **10** toward **6-CZGNR-(2,1)**. The presence of delocalized electrons in the core of GNR increases the ^1H line widths significantly due to paramagnetic relaxation effects. A less π -stacking of the GNR core can be further identified by the 2D $^1\text{H}-^1\text{H}$ DQ-SQ NMR correlation spectra, showing a reduced spread of the $^1\text{H}-^1\text{H}$ autocorrelation signals between the aromatic protons (only up to $\sim 12 \text{ ppm}$), compared to those planar GNRs with stronger $\pi-\pi$ interactions (up to $\sim 15 \text{ ppm}$).^{27,32,33}

Optical Properties of **2, **3**, and **6-CZGNR-(2,1)**.** Thanks to the curved geometry and the dodecyl chains installed on the

edges, the 6-CZGNR-(2,1) could be easily dispersed upon sonication in common organic solvents, such as *N*-methyl-2-pyrrolidone (NMP) and tetrahydrofuran. Interestingly, the same nonplanarity seems to be responsible for the weak affinity of GNRs to form ordered structures on HOPG and Au(111): in all of our experiments, only empty surface, unstructured aggregates, or previously reported contaminants^{34,35} were observed (Figures S12–S15). As shown in Figure 3d, the UV–vis absorption spectrum of 6-CZGNR-(2,1) was recorded in NMP (0.1 mg/mL) and compared with that of model compounds 2 and 3 in CH₂Cl₂ solution (1×10^{-5} M). For model compounds 2 and 3, the absorption peaks with the longest wavelength occur at 475 and 544 nm, respectively, which are in excellent agreement with the result of time-dependent DFT calculations (Figure S22 and Table S8). Compared to 2 and 3, the absorption of 6-CZGNR-(2,1) in NMP solution displays a considerable red-shift into the near-infrared (NIR) region with a large and broad absorption peak at ~ 835 nm. The optical bandgap of 6-CZGNR-(2,1) is estimated to be 0.99 eV from the onset of the absorption (1250 nm), which is a record-low value compared with those of reported solution-phase processable GNRs.^{20,23–25} The difference between the experimental and computed absorption spectra for 6-CZGNR-(2,1) (computed for the tetramer) is small with the longest calculated wavelength lying at 1349 nm, in very good agreement with the measured value. The first excited state is associated with a strong HOMO to LUMO transition (Table S9) for all the studied structures.

THz Study of 6-CZGNR-(2,1). To study the charge transport properties of 6-CZGNR-(2,1), we employed contact-free, optical-pump THz-probe (OPTP) spectroscopy.^{36,37} In OPTP measurements, charge carriers are generated via photoexciting a drop-casted film of 6-CZGNR-(2,1) by a 3.10 eV laser pulse. The complex conductivity of the photogenerated charge carriers is subsequently probed by a single-cycle THz pulse. As shown in Figure 4a, we observed a rapid, subpico-

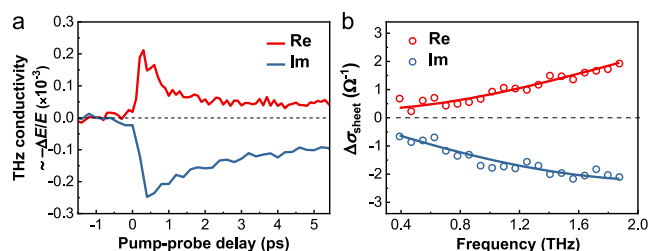


Figure 4. (a) Time-resolved terahertz real and imaginary parts of the photoconductivity (proportional to the relative changes in the transmitted field, $-\Delta E/E$) of 6-CZGNR-(2,1) following photoexcitation. (b) The frequency-resolved THz complex conductivity, measured 0.8 ps after photoexcitation. Lines indicate the Drude-Smith fit.

second rise in the real conductivity, reflecting the photo-generation of free charges in the 6-CZGNR-(2,1). The subsequent rapid decay can be attributed to carrier trapping, and/or the formation of bound electron–hole pairs, that is, exciton formation. Both the real and imaginary conductivity dynamics are fully consistent with the previous results for other GNRs.^{20,21,39} Furthermore, the frequency-resolved THz conductivity at ~ 0.8 ps after photoexcitation is shown in Figure 4b. The Drude-Smith (DS) model can well describe the conductivity response (see details in SI), where the transport

of free charges is assumed to experience backscattering processes due to, for example, structural deformation and conjugational defects.^{38,39} In the DS model, a parameter c represents the backscattering probability for carrier transport, and the value of c ranges from 0 (free charge) to -1 (preferential backscattering). From the DS fitting, we obtained the DS charge scattering time τ to be 29 ± 2 fs, as well as the backscattering rate c to be -0.97 ± 0.01 . This yields the macroscopic charge mobility (μ_{macro}) for the thin film to be $\sim 18 \text{ cm}^2 \text{ V}^{-1} \text{ s}^{-1}$ by taking into account the backscattering contribution: $\mu_{\text{macro}} = \mu(1 + c)$. The μ_{macro} mobility of the 6-CZGNR-(2,1) thin film is among the highest reported values for the GNRs thin film.²⁰ Note that this relatively high inferred charge carrier mobility originates primarily from the small effective mass of the unique GNRs. The DS charge scattering time determined here is very similar to the values (~ 30 fs) previously reported for various other GNRs.³⁷

CONCLUSION

In summary, we have demonstrated a new family of curved GNRs containing periodic cove-zigzag edge structures, namely *N*-CZGNR-(*n,m*). Apart from the topological nonplanar geometry induced by the cove unit along both edges of the resultant GNRs, the bandgap of such GNRs can be readily tuned from semiconducting to near-metallic by varying the parameters n and m . Moreover, we present the first synthesis of a periodic cove-zigzag edged GNRs (6-CZGNR-(2,1)) through two-step solution synthesis from a S-shaped key monomer (1). Remarkably, the achieved 6-CZGNR-(2,1) exhibits a record-narrow optical bandgap of 0.99 eV and a small effective mass, which results in high carrier mobility of up to $20 \text{ cm}^2 \text{ V}^{-1} \text{ s}^{-1}$. Therefore, our study opens a door for the synthesis of curved GNRs through the incorporation of periodic cove units along the zigzag-edged GNR backbone and will largely increase the members of the cove-edged GNR family available for diverse GNR-based device studies.

EXPERIMENTAL SECTION

The full experimental details and characterization methods can be found in the Supporting Information.

ASSOCIATED CONTENT

Supporting Information

The Supporting Information is available free of charge at <https://pubs.acs.org/doi/10.1021/jacs.1c09000>.

Synthetic procedures and characterization data, additional optical, FTIR and Raman spectra of model compounds, STM and AFM characterizations, solid-state NMR analysis, DFT calculation details, terahertz spectroscopy, and NMR and mass spectra of new compounds (PDF)

Assignment of the IR spectrum of compound 3 (CH out-of-plane bending) (MP4)

AUTHOR INFORMATION

Corresponding Authors

Ji Ma – Centre for Advancing Electronics Dresden (cfaed) and Faculty of Chemistry and Food Chemistry, Technische Universität Dresden, 01062 Dresden, Dresden, Germany; Email: ji.ma@tu-dresden.de

Junzhi Liu – Department of Chemistry and State Key Laboratory of Synthetic Chemistry, The University of Hong

Kong, Hong Kong, China; orcid.org/0000-0001-7146-0942; Email: juliu@hku.hk

Xinliang Feng – Centre for Advancing Electronics Dresden (cfaed) and Faculty of Chemistry and Food Chemistry, Technische Universität Dresden, 01062 Dresden, Germany; Max Planck Institute of Microstructure Physics, Halle 06120, Germany; orcid.org/0000-0003-3885-2703; Email: xinliang.feng@tu-dresden.de

Authors

Xu Wang – College of Polymer Science and Engineering, State Key Laboratory of Polymer Material and Engineering, Sichuan University, 610065 Chengdu, P.R. China; Centre for Advancing Electronics Dresden (cfaed) and Faculty of Chemistry and Food Chemistry, Technische Universität Dresden, 01062 Dresden, Germany; orcid.org/0000-0001-7162-7052

Wenhao Zheng – Max Planck Institute for Polymer Research, 55128 Mainz, Germany

Silvio Osella – Chemical and Biological Systems Simulation Lab, Centre of New Technologies, University of Warsaw, 02-097 Warsaw, Poland; orcid.org/0000-0001-8541-1914

Nicolás Arisnabarreta – Department of Chemistry, Division of Molecular Imaging and Photonics, KU Leuven, 3001 Leuven, Belgium

Jörn Droste – Institute of Physical Chemistry, Westfälische Wilhelms-Universität Münster, D-48149 Münster, Germany

Gianluca Serra – Dipartimento di Chimica, Materiali ed Ingegneria Chimica “G. Natta”, Politecnico di Milano, 20133 Milano, Italy

Oleksandr Ivasenko – Department of Chemistry, Division of Molecular Imaging and Photonics, KU Leuven, 3001 Leuven, Belgium

Andrea Lucotti – Dipartimento di Chimica, Materiali ed Ingegneria Chimica “G. Natta”, Politecnico di Milano, 20133 Milano, Italy

David Beljonne – Laboratory for Chemistry of Novel Materials, Université de Mons, B-7000 Mons, Belgium; orcid.org/0000-0002-2989-3557

Mischa Bonn – Max Planck Institute for Polymer Research, 55128 Mainz, Germany; orcid.org/0000-0001-6851-8453

Xiangyang Liu – College of Polymer Science and Engineering, State Key Laboratory of Polymer Material and Engineering, Sichuan University, 610065 Chengdu, P.R. China; orcid.org/0000-0002-9246-3437

Michael Ryan Hansen – Institute of Physical Chemistry, Westfälische Wilhelms-Universität Münster, D-48149 Münster, Germany; orcid.org/0000-0001-7114-8051

Matteo Tommasini – Dipartimento di Chimica, Materiali ed Ingegneria Chimica “G. Natta”, Politecnico di Milano, 20133 Milano, Italy; orcid.org/0000-0002-7917-426X

Steven De Feyter – Department of Chemistry, Division of Molecular Imaging and Photonics, KU Leuven, 3001 Leuven, Belgium; orcid.org/0000-0002-0909-9292

Hai I. Wang – Max Planck Institute for Polymer Research, 55128 Mainz, Germany; orcid.org/0000-0003-0940-3984

Complete contact information is available at:
<https://pubs.acs.org/10.1021/jacs.1c09000>

Author Contributions

The manuscript was written through contributions of all authors. All authors have given approval to the final version of the manuscript.

Notes

The authors declare no competing financial interest.

ACKNOWLEDGMENTS

X.W. is grateful for the National Natural Science Foundation of China (Grants 51803129, 51633004) and the International Visiting Program for Excellent Young Scholars of SCU. This research was financially supported by the EU Graphene Flagship (Graphene Core 3, 881603), ERC Consolidator Grant (T2DCP, 819698), the Center for Advancing Electronics Dresden (cfaed) and the DFG-SNSF Joint Switzerland-German Research Project (EnhanTopo, No. 429265950). S.O. acknowledges the computational resources of the Interdisciplinary Center for Mathematical and Computational Modelling (ICM, University of Warsaw) under the G53-8 and G83-28 computational grants. J.L. is grateful for the funding support from Hong Kong Research Grants Council (HKU 27301720) and ITC to the SKL. G.S. and M.T. acknowledge funding by the Italian Ministry of Education, Universities and Research (MIUR) through the PRIN 2017 program (Project No. 2017PJ5XXX “MAGIC DUST”). J.D. thanks the DFG for funding (SFB 858). S.D.F. acknowledges the financial support from ULTIMATE-H2020-MSCA-ITN-2018 (Grant Agreement 813036). S.D.F., N.A., and O.I. acknowledge financial support from KU Leuven and FWO. Computational resources in Mons were provided by the Consortium des Équipements de Calcul Intensif (CÉCI), funded by the Fonds de la Recherche Scientifiques de Belgique (F.R.S.-FNRS) under Grant 2.5020.11, as well as the Tier-1 supercomputer of the Federation Wallonie-Bruxelles, infrastructure funded by the Walloon Region under Grant Agreement 1117545. D.B. is a FNRS Research Director.

REFERENCES

- (1) Narita, A.; Wang, X. Y.; Feng, X.; Müllen, K. New Advances in Nanographene Chemistry. *Chem. Soc. Rev.* **2015**, *44*, 6616–6643.
- (2) Cai, J.; Ruffieux, P.; Jaafar, R.; Bieri, M.; Braun, T.; Blankenburg, S.; Muoth, M.; Seitsonen, A. P.; Saleh, M.; Feng, X.; Müllen, K.; Fasel, R. Atomically Precise Bottom-up Fabrication of Graphene Nanoribbons. *Nature* **2010**, *466*, 470–473.
- (3) Kolmer, M.; Steiner, A.; Izydorczyk, I.; Ko, W.; Englund, M.; Szymonski, M.; Li, A.; Amsharov, K. Rational Synthesis of Atomically Precise Graphene Nanoribbons Directly on Metal Oxide Surfaces. *Science* **2020**, *369*, 571–575.
- (4) Saraswat, V.; Jacobberger, R. M.; Arnold, M. S. Materials Science Challenges to Graphene Nanoribbon Electronics. *ACS Nano* **2021**, *15*, 3674–3708.
- (5) Ruffieux, P.; Wang, S.; Yang, B.; Sánchez-Sánchez, C.; Liu, J.; Dienel, T.; Talirz, L.; Shinde, P.; Pignedoli, C. A.; Passerone, D.; Dumslaff, T.; Feng, X.; Müllen, K.; Fasel, R. On-surface Synthesis of Graphene Nanoribbons with Zigzag Edge Topology. *Nature* **2016**, *531*, 489–492.
- (6) Chen, L.; Hernandez, Y.; Feng, X.; Müllen, K. From Nanographene and Graphene Nanoribbons to Graphene Sheets: Chemical Synthesis. *Angew. Chem., Int. Ed.* **2012**, *51*, 7640–7654.
- (7) Liu, J.; Feng, X. Synthetic Tailoring of Graphene Nanostructures with Zigzag-Edged Topologies: Progress and Perspectives. *Angew. Chem., Int. Ed.* **2020**, *59*, 23386–23401.
- (8) Chen, Z.; Narita, A.; Müllen, K. Graphene Nanoribbons: On-Surface Synthesis and Integration into Electronic Devices. *Adv. Mater.* **2020**, *32*, 2001893.

- (9) Narita, A.; Chen, Z.; Chen, Q.; Müllen, K. Solution and on-Surface Synthesis of Structurally Defined Graphene Nanoribbons as a New Family of Semiconductors. *Chem. Sci.* **2019**, *10*, 964–975.
- (10) Niu, W.; Liu, J.; Mai, Y.; Müllen, K.; Feng, X. Synthetic Engineering of Graphene Nanoribbons with Excellent Liquid-Phase Processability. *Trends Chem.* **2019**, *1*, 549–558.
- (11) Jolly, A.; Miao, D.; Daigle, M.; Morin, J. F. Emerging Bottom-Up Strategies for the Synthesis of Graphene Nanoribbons and Related Structures. *Angew. Chem., Int. Ed.* **2020**, *59*, 4624–4633.
- (12) Liu, J.; Li, B.; Tan, Y.; Giannakopoulos, A.; Sanchez-Sanchez, C.; Beljonne, D.; Ruffieux, P.; Fasel, R.; Feng, X.; Müllen, K. Toward Cove-Edged Low Band Gap Graphene Nanoribbons. *J. Am. Chem. Soc.* **2015**, *137*, 6097–6103.
- (13) Lee, Y.; Zhao, F.; Cao, T.; Ihm, J.; Louie, S. G. Topological Phases in Cove-Edged and Chevron Graphene Nanoribbons: Geometric Structures, $Z(2)$ Invariants, and Junction States. *Nano Lett.* **2018**, *18*, 7247–7253.
- (14) Bheemireddy, S. R.; Hautzinger, M. P.; Li, T.; Lee, B.; Plunkett, K. N. Conjugated Ladder Polymers by a Cyclopentannulation Polymerization. *J. Am. Chem. Soc.* **2017**, *139*, 5801–5807.
- (15) Sisto, T. J.; Zhong, Y.; Zhang, B.; Trinh, M. T.; Miyata, K.; Zhong, X.; Zhu, X. Y.; Steigerwald, M. L.; Ng, F.; Nuckolls, C. Long, Atomically Precise Donor–Acceptor Cove-Edge Nanoribbons as Electron Acceptors. *J. Am. Chem. Soc.* **2017**, *139*, 5648–5651.
- (16) Liu, F.; Shen, X.; Wu, Y.; Bai, L.; Zhao, H.; Ba, X. Synthesis of Ladder-Type Graphene Ribbon Oligomers from Pyrene Units. *Tetrahedron Lett.* **2016**, *57*, 4157–4161.
- (17) Gröning, O.; Wang, S.; Yao, X.; Pignedoli, C. A.; Borin Barin, G.; Daniels, C.; Cupo, A.; Meunier, V.; Feng, X.; Narita, A.; Müllen, K.; Ruffieux, P.; Fasel, R. Engineering of Robust Topological Quantum Phases in Graphene Nanoribbons. *Nature* **2018**, *560*, 209–213.
- (18) Rizzo, D. J.; Veber, G.; Cao, T.; Bronner, C.; Chen, T.; Zhao, F.; Rodriguez, H.; Louie, S. G.; Crommie, M. F.; Fischer, F. R. Topological Band Engineering of Graphene Nanoribbons. *Nature* **2018**, *560*, 204–208.
- (19) Li, Y.; Zhou, Z.; Shen, P.; Chen, Z. Electronic and Magnetic Properties of Hybrid Graphene Nanoribbons with Zigzag-Armchair Heterojunctions. *J. Phys. Chem. C* **2012**, *116*, 208–213.
- (20) Niu, W.; Ma, J.; Soltani, P.; Zheng, W.; Liu, F.; Popov, A. A.; Weigand, J. J.; Komber, H.; Poliani, E.; Casiraghi, C.; Droste, J.; Hansen, M. R.; Osella, S.; Beljonne, D.; Bonn, M.; Wang, H. I.; Feng, X.; Liu, J.; Mai, Y. A Curved Graphene Nanoribbon with Multi-Edge Structure and High Intrinsic Charge Carrier Mobility. *J. Am. Chem. Soc.* **2020**, *142*, 18293–18298.
- (21) Yao, X.; Zheng, W.; Osella, S.; Qiu, Z.; Fu, S.; Schollmeyer, D.; Müller, B.; Beljonne, D.; Bonn, M.; Wang, H. I.; Müllen, K.; Narita, A. Synthesis of Nonplanar Graphene Nanoribbon with Fjord Edges. *J. Am. Chem. Soc.* **2021**, *143*, 5654–5658.
- (22) Fu, Y.; Yang, H.; Gao, Y.; Huang, L.; Berger, R.; Liu, J.; Lu, H.; Cheng, Z.; Du, S.; Gao, H. J.; Feng, X. On-Surface Synthesis of NBN-Doped Zigzag-Edged Graphene Nanoribbons. *Angew. Chem.* **2020**, *132*, 8958–8964.
- (23) Yang, W.; Lucotti, A.; Tommasini, M.; Chalifoux, W. A. Bottom-Up Synthesis of Soluble and Narrow Graphene Nanoribbons Using Alkyne Benzannulations. *J. Am. Chem. Soc.* **2016**, *138*, 9137–9144.
- (24) Li, G.; Yoon, K.; Zhong, X.; Wang, J.; Zhang, R.; Guest, J. R.; Wen, J.; Zhu, X. Y.; Dong, G. A Modular Synthetic Approach for Band-Gap Engineering of Armchair Graphene Nanoribbons. *Nat. Commun.* **2018**, *9*, 1687.
- (25) Kim, K. T.; Jung, J. W.; Jo, W. H. Synthesis of Graphene Nanoribbons with Various Widths and Its Application to Thin-film Transistor. *Carbon* **2013**, *63*, 202–209.
- (26) Yazyev, O. V. A Guide to the Design of Electronic Properties of Graphene Nanoribbons. *Acc. Chem. Res.* **2013**, *46*, 2319–2328.
- (27) Narita, A.; Feng, X.; Hernandez, Y.; Jensen, S. A.; Bonn, M.; Yang, H.; Verzhbitskiy, I. A.; Casiraghi, C.; Hansen, M. R.; Koch, A. H. R.; Fytas, G.; Ivashenko, O.; Li, B.; Mali, K. S.; Balandina, T.; Mahesh, S.; De Feyter, S.; Müllen, K. Synthesis of Structurally Well-Defined and Liquid-phase-Processable Graphene Nanoribbons. *Nat. Chem.* **2014**, *6*, 126.
- (28) Negri, F.; Castiglioni, C.; Tommasini, M.; Zerbi, G. A Computational Study of the Raman Spectra of Large Polycyclic Aromatic Hydrocarbons: Toward Molecularly Defined Subunits of Graphite. *J. Phys. Chem. A* **2002**, *106*, 3306–3317.
- (29) Verzhbitskiy, I. A.; Corato, M. D.; Ruini, A.; Molinari, E.; Narita, A.; Hu, Y.; Schwab, M. G.; Bruna, M.; Yoon, D.; Milana, S.; Feng, X.; Müllen, K.; Ferrari, A. C.; Casiraghi, C.; Prezzi, D. Raman Fingerprints of Atomically Precise Graphene Nanoribbons. *Nano Lett.* **2016**, *16*, 3442–3447.
- (30) Gillen, R.; Mohr, M.; Maultzsch, J. Symmetry Properties of Vibrational Modes in Graphene Nanoribbons. *Phys. Rev. B: Condens. Matter Mater. Phys.* **2010**, *81*, 205426.
- (31) Castiglioni, C.; Mapelli, C.; Negri, F.; Zerbi, G. Origin of the D line in the Raman spectrum of graphite: A Study Based on Raman Frequencies and Intensities of Polycyclic Aromatic Hydrocarbon Molecules. *J. Chem. Phys.* **2001**, *114*, 963–974.
- (32) Narita, A.; Verzhbitskiy, I. A.; Frederickx, W.; Mali, K. S.; Jensen, S. A.; Hansen, M. R.; Bonn, M.; De Feyter, S.; Casiraghi, C.; Feng, X.; Müllen, K. Bottom-Up Synthesis of Liquid-Phase-Processable Graphene Nanoribbons with Near-Infrared Absorption. *ACS Nano* **2014**, *8*, 11622–11630.
- (33) Xu, F.; Yu, C.; Tries, A.; Zhang, H.; Kläui, M.; Basse, K.; Hansen, M. R.; Bilbao, N.; Bonn, M.; Wang, H. I.; Mai, Y. Tunable Superstructures of Dendronized Graphene Nanoribbons in Liquid Phase. *J. Am. Chem. Soc.* **2019**, *141*, 10972–10977.
- (34) Gallagher, P.; Lee, M.; Amet, F.; Maksymovych, P.; Wang, J.; Wang, S.; Lu, X.; Zhang, G.; Watanabe, K.; Taniguchi, T.; Goldhaber-Gordon, D. Switchable Friction Enabled by Nanoscale Self-Assembly on Graphene. *Nat. Commun.* **2016**, *7*, 10745.
- (35) Seibert, S.; Klassen, S.; Latus, A.; Bechstein, R.; Kühnle, A. Origin of Ubiquitous Stripes at the Graphite–Water Interface. *Langmuir* **2020**, *36*, 7789–7794.
- (36) Ulbricht, R.; Hendry, E.; Shan, J.; Heinz, T. F.; Bonn, M. Carrier Dynamics in Semiconductors Studied with Time-Resolved Terahertz Spectroscopy. *Rev. Mod. Phys.* **2011**, *83*, 543.
- (37) Tries, A.; Osella, S.; Zhang, P.; Xu, F.; Ramanan, C.; Kläui, M.; Mai, Y.; Beljonne, D.; Wang, H. I. Experimental Observation of Strong Exciton Effects in Graphene Nanoribbons. *Nano Lett.* **2020**, *20*, 2993–3002.
- (38) Jensen, S. A.; Ulbricht, R.; Narita, A.; Feng, X.; Müllen, K.; Hertel, T.; Turchinovich, D.; Bonn, M. Ultrafast Photoconductivity of Graphene Nanoribbons and Carbon Nanotubes. *Nano Lett.* **2013**, *13*, 5925–5930.
- (39) Ivanov, I.; Hu, Y.; Osella, S.; Beser, U.; Wang, H. I.; Beljonne, D.; Narita, A.; Müllen, K.; Turchinovich, D.; Bonn, M. Role of Edge Engineering in Photoconductivity of Graphene Nanoribbons. *J. Am. Chem. Soc.* **2017**, *139*, 7982–7988.